

Nonlinear demixed component analysis for neural population data as a low-rank kernel regression problem

Author: Kenneth W. Latimer^{1*}

¹Department of Neurobiology, University of Chicago

*Correspondence; E-mail: latimerk@uchicago.edu.

March 22, 2022

Here I introduce an extension to demixed principal component analysis (dPCA), a linear dimensionality reduction technique for analyzing the activity of neural populations, to the case of nonlinear components. This extension, kernel demixed principal component analysis (kdPCA), relies on kernel least-squares regression techniques, and it resembles kernel-based extensions to standard principal component analysis and canonical correlation analysis. kdPCA includes dPCA as a special case when the kernel is linear. I present simulated examples of high-dimensional neural activity generated from low-dimensional trajectories and compare the results of kdPCA to dPCA. These simulations demonstrate that neurally relevant nonlinearities - such as stimulus-dependent gain and rotations - impede the ability of dPCA to demix neural activity corresponding to experimental parameters. However, kdPCA can still recover interpretable components from such data. Additionally, I apply kdPCA to a neural population previously analyzed by dPCA from rat orbitofrontal cortex during an odor classification task in recovering decision-related activity. The components recovered by kdPCA achieve better generalization and demixing performance compared to dPCA by accounting for a nonlinear interaction between stimulus and decision in the neural activity. In conclusion, simple nonlinear interactions inhibit the ability of linear dimensionality reduction techniques to recover interpretable demixed components in neural data, but this problem can be tackled by nonlinear dimensionality reduction approaches like kdPCA.

1 Introduction

Dimensionality reduction has become an essential step for analyzing large-scale neural recordings (Cunningham & Byron, 2014; Gao & Ganguli, 2015; Williamson et al., 2018). Recent work on dimensionality reduction has focused on methods to discover components of neural activity which are aligned to experimental variables of interest, such as animal behavior and stimulus

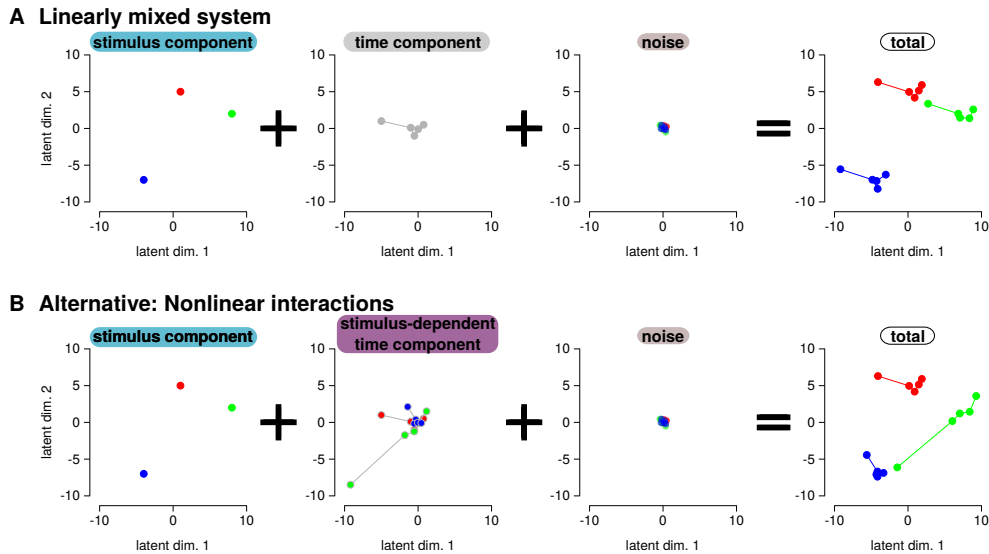


Figure 1: Two dimensional subspaces representing latent neural activity. **(A)** In this example, neural activity is the sum of the component stimulus, a time component, and independent noise. The right panel shows the total signal, and each color corresponds to a stimulus condition. See similar example in Figure 2 of Kobak et al. (2016). **(B)** In this example, the time component is the same as in A. However, the time component is stretched and rotated depending on the stimulus (rather than only translated).

condition (Kobak et al., 2016; Williams et al., 2018). Here, I focus on one particular method, demixed PCA, proposed by Kobak et al. (2016). A key assumption of this method is that components can be combined linearly to produce a low-dimensional representation of observed neural activity (**Fig 1A**). However, it is likely the case in real data that experimental parameters can interact nonlinearly. For example, the trajectories in neural space could be scaled (as with stimulus-dependent gain) and rotated for each stimulus while still maintaining separability in the low-dimensional space (**Fig 1B**). Although dPCA considers interaction components to account for such dependencies, dPCA may still fail to recover components that depend solely on particular a task parameter (i.e., fails to demix parameters) because dPCA is restricted to linear projections. However, it may be possible to find a low-dimensional set of nonlinear components that successfully demix the neural activity contributed by each task parameter.

I present an extension to dPCA to find nonlinear task-related components. This method is related to kernel-based extensions of standard principal component analysis (PCA) (Schölkopf et al., 1998), canonical correlation analysis (CCA) (Lai & Fyfe, 2000; Haroon et al., 2004; Rodu et al., 2018), and kernel regularized least-squares regression (Hainmueller & Hazlett, 2014). In this method, the data points are projected from neural activity space (\mathbb{R}^N) into a potentially higher-dimensional space (\mathcal{A}). Using a standard kernel approach with low-rank matrix approximations, kdPCA recovers a low-dimensional subspace in \mathcal{A} that represents the high-dimensional neural activity while demixing the task variables. I demonstrate the utility of this method using several simulations and compare to dPCA. Finally, I apply kdPCA to a population of neurons recorded from rate orbitofrontal cortex (OFC) during an odor classification

task (Kepecs et al., 2008; Uchida et al., 2016; Kobak et al., 2016).

2 Methods

2.1 dPCA

This section briefly describes dPCA from Kobak et al. (2016). The responses of N neurons are placed in a matrix of observations, \mathbf{X} , of size $M \times N$. The number of observations, M , is the total number of time points over all conditions (or trials). For simplicity, I assume that the responses of each neuron have mean 0 (that is, the mean of each column of \mathbf{X} is 0). Each row of \mathbf{X} can be indexed by different experimental parameters. For brevity, I consider only 2 parameters here: time and stimulus. Let the row vector $\mathbf{X}_{(t,s)} \in \mathbb{R}^N$ be the observed activity at time t for stimulus s . The observations can then be decomposed as the sum of averages over conditions plus an interaction (which possibly includes noise) term

$$\mathbf{X}_{(t,s)} = \overline{\mathbf{X}_{(\cdot,s)}} + \overline{\mathbf{X}_{(t,\cdot)}} + \overline{\mathbf{X}_{(\cdot,\cdot)}} \quad (1)$$

where the averages over parameters are

$$\overline{\mathbf{X}_{(\cdot,s)}} = \langle \mathbf{X}_{(t,s)} \rangle_t \quad (2)$$

$$\overline{\mathbf{X}_{(t,\cdot)}} = \langle \mathbf{X}_{(t,s)} \rangle_s \quad (3)$$

$$\overline{\mathbf{X}_{(\cdot,\cdot)}} = \mathbf{X}_{(t,s)} - \overline{\mathbf{X}_{(\cdot,s)}} - \overline{\mathbf{X}_{(t,\cdot)}}. \quad (4)$$

This decomposition could be extended to include other indices such as trial and decision as shown in Kobak *et al.*

The next step is to construct the matrices \mathbf{X}_S , \mathbf{X}_T , and \mathbf{X}_{ST} (each of size $M \times N$) by replacing the rows of \mathbf{X} with the averaged terms

$$\mathbf{X}_{S,(t,s)} = \overline{\mathbf{X}_{(\cdot,s)}} \quad (5)$$

$$\mathbf{X}_{T,(t,s)} = \overline{\mathbf{X}_{(t,\cdot)}} \quad (6)$$

$$\mathbf{X}_{ST,(t,s)} = \overline{\mathbf{X}_{(\cdot,\cdot)}} \quad (7)$$

$$(8)$$

The goal of dPCA is to find a low-rank reconstruction of \mathbf{X} by obtaining low-rank reconstructions of the time component (\mathbf{X}_T), the stimulus component (\mathbf{X}_S), and the interaction component (\mathbf{X}_{ST}) and then summing the result. The parameters t and s are indexed by $\gamma \in \{t, s, st\}$.

More formally, dPCA finds matrices \mathbf{D}_γ and \mathbf{F}_γ of size $N \times R_\gamma$ where $R_\gamma \ll N$ that minimize the quantity

$$L_{dPCA} = \sum_{\gamma \in \{t,s,st\}} \|\mathbf{X}_\gamma - \mathbf{X} \mathbf{D}_\gamma \mathbf{F}_\gamma^\top\|^2 + \mu \|\mathbf{D}_\gamma \mathbf{F}_\gamma^\top\|^2 \quad (9)$$

where and $\|\cdot\|$ is the Frobenius norm. The regularization term, μ , is a function of the variable λ :

$$\mu = \frac{\lambda}{M} \|\mathbf{X}\|^2. \quad (10)$$

(This term differs slightly from Kobak *et al.* who set $\mu = (\lambda\|\mathbf{X}\|)^2$.)

Solving for \mathbf{F}_γ is accomplished by setting

$$\mathbf{C}_\gamma = \mathbf{D}_\gamma \mathbf{F}_\gamma \quad (11)$$

and then taking the regularized least-squares solution where \mathbf{I}_N is the $N \times N$ identity matrix:

$$\mathbf{C}_\gamma = (\mathbf{X}^\top \mathbf{X} + \lambda \mathbf{I}_N)^{-1} \mathbf{X}^\top \mathbf{X}_\gamma. \quad (12)$$

Kobak *et al.* complete the reduced-rank regression by performing PCA on $\mathbf{X}\mathbf{C}_\gamma$, taking the first R principal components (\mathbf{U}_R), and setting

$$\mathbf{D}_\gamma = \mathbf{C}_\gamma \mathbf{U}_R \quad (13)$$

$$\mathbf{F}_\gamma = \mathbf{U}_R^\top. \quad (14)$$

The procedure is repeated for all γ .

2.2 kdPCA

To build upon dPCA, each observation (the activity of N neurons in one time bin) is mapped into a new, possibly higher-dimensional space, by a function

$$\Psi : \mathbb{R}^N \rightarrow \mathcal{A}. \quad (15)$$

The term $\Psi(\mathbf{X})$ denotes the matrix obtained by passing each row of \mathbf{X} through Ψ . This new matrix is then used to reconstruct the same decomposition of X used by dPCA. kdPCA finds linear operators \mathbf{H}_γ that project the terms of $\Psi(X)$ into a low-dimensional space (\mathbb{R}_γ^R) and matrices \mathbf{G}_γ that reconstructs the parameter-dependent observations, \mathbf{X}_γ .

For a concrete example of one possible choice of Ψ , **Fig 2 left** shows the activity of two neurons (x and y) over several trials in two stimulus categories (blue and red). In the neural activity space, \mathbb{R}^2 , the two stimulus categories cannot be linearly separated: no straight line can divide the red and blue points and standard PCA cannot find a subspace that separates the two classes. Let $\Psi_{ex} : \mathbb{R}^2 \rightarrow \mathbb{R}^3$ be a polynomial expansion of the original space such that:

$$\Psi_{ex}(x, y) = (x, y, x^2 + y^2) \quad (16)$$

In this transformed space, **Fig 2B** shows that the conditions can now be separated linearly. Additionally, performing PCA in this higher dimensional space reveals a single component that separates the red and blue classes (Schölkopf et al., 1998). Thus, taking nonlinear functions of the neural activity can reveal components related to different experimental conditions that cannot be seen by purely linear methods.

Plugging Ψ into the dPCA loss function produces the analogous loss function for kdPCA:

$$L_{kdPCA} = \sum_{\gamma \in \{t, s, st\}} \|\mathbf{X}_\gamma - \Psi(\mathbf{X})\mathbf{G}_\gamma \mathbf{H}_\gamma^\top\|^2 + \eta \|\mathbf{G}_\gamma \mathbf{H}_\gamma^\top\|^2 \quad (17)$$

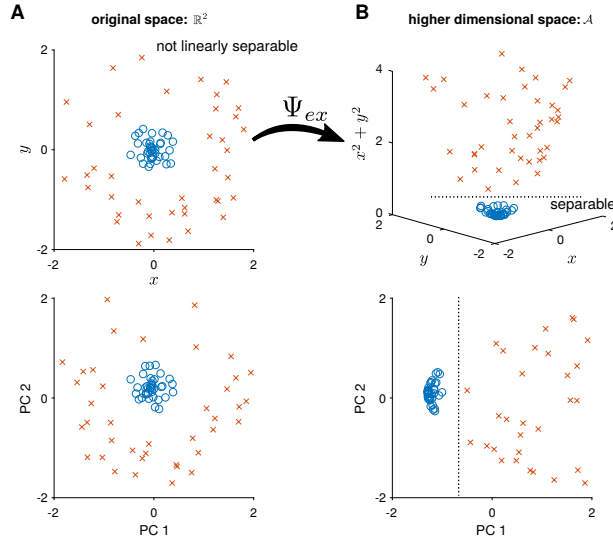


Figure 2: **A** (top) A two dimensional space of neural activity. Each color represents two possible conditions. In this space, the red and blue conditions cannot be linearly separated. Performing PCA (bottom) in the original space returns essentially the same representation. This situation could potentially occur in a neural population exhibiting rotational dynamics with a different gain across conditions. **B** Projecting these observations into a higher dimensional space (top) through the function Ψ allows these classes to be linearly separable. In this higher dimensional space, the two classes are separated in the first principle component (bottom).

where the columns R_γ of \mathbf{H}_γ are in \mathcal{A} . The regularization term, η , is a function of lambda:

$$\eta = \lambda \frac{1}{M} \text{trace}(\mathbf{K}). \quad (18)$$

As with \mathbf{F}_γ in dPCA, \mathbf{G}_γ is a matrix of size $N \times R_\gamma$. The parameter λ again controls the strength of the regularization term.

Each column of \mathbf{H} must be in the row space of $\Psi(\mathbf{X})$ (otherwise the weights will be outside the subspace of \mathcal{A} explored in the data). Therefore, for some matrix \mathbf{Z}_γ of size $N \times R_\gamma$

$$\mathbf{G}_\gamma = \Psi(\mathbf{X})^\top \mathbf{Z}_\gamma. \quad (19)$$

Plugging eq. 19 into eq. 17 gives

$$L_{kdPCA} = \sum_{\gamma \in \{t, s, st\}} \|\mathbf{X}_\gamma - \Psi(\mathbf{X})\Psi(\mathbf{X})^\top \mathbf{Z}_\gamma \mathbf{H}_t^\top\|^2 + \eta \|\mathbf{G}_\gamma \mathbf{H}_\gamma^\top\|^2. \quad (20)$$

The the elements of the matrix $\Psi(\mathbf{X})\Psi(\mathbf{X})^\top$ are dot products of rows of $\Psi(\mathbf{X})$, which can be rewritten using a kernel function κ on the rows of \mathbf{X} :

$$\mathbf{K}_{i,j} = (\Psi(\mathbf{X})\Psi(\mathbf{X})^\top)_{i,j} = (\Psi(\mathbf{X})_{i,\cdot} \cdot \Psi(\mathbf{X})_{j,\cdot}) = \kappa(\mathbf{X}_{i,\cdot}, \mathbf{X}_{j,\cdot}) \quad (21)$$

where $\mathbf{X}_{j,\cdot}$ is the j th row of \mathbf{X} . This results in the loss function

$$L_{kdPCA} = \sum_{\gamma \in \{t, s, st\}} \|\mathbf{X}_\gamma - \mathbf{K} \mathbf{Z}_\gamma \mathbf{H}_\gamma^\top\|^2 + \eta \|\mathbf{G}_\gamma \mathbf{H}_\gamma^\top\|^2. \quad (22)$$

To solve for \mathbf{Z}_γ and \mathbf{H}_γ , the same low-rank regression procedure used for dPCA is applied. First, the full-rank regularized least-squares solution is (Hainmueller & Hazlett, 2014):

$$\mathbf{C}_\gamma = (\mathbf{K} + \eta \mathbf{I}_M)^{-1} \mathbf{X}_\gamma. \quad (23)$$

Reduced-rank regression is then completed by performing PCA on $\mathbf{X}\mathbf{C}_\gamma$, taking the first R principal components (\mathbf{U}_R), and setting

$$\mathbf{Z}_\gamma = \mathbf{C}_\gamma \mathbf{U}_R \quad (24)$$

$$\mathbf{H}_\gamma = \mathbf{U}_R^\top. \quad (25)$$

The procedure is repeated for all γ .

To project a new observation, \mathbf{x}^* , into the low-dimensional space for parameter γ , applying eq. 19 and the kernel representation shows

$$\Psi(\mathbf{x}^*) \mathbf{G}_\gamma = \Psi(\mathbf{x}^*) \Psi(\mathbf{X})^\top \mathbf{Z}_\gamma \quad (26)$$

$$= \mathbf{k}^* \mathbf{Z}_\gamma \quad (27)$$

where \mathbf{k}^* is a row vector of length N where each element is

$$\mathbf{k}_i^* = \kappa(\mathbf{x}^*, \mathbf{X}_i, \cdot). \quad (28)$$

For the examples here, I use a linear kernel and a Gaussian kernel

$$\kappa_{lin}(\mathbf{x}, \mathbf{y}) = \mathbf{x} \cdot \mathbf{y} \quad (29)$$

$$\kappa_{Gauss}(\mathbf{x}, \mathbf{y}) = \exp\left(-\frac{1}{2l^2}((\mathbf{x} - \mathbf{y}) \cdot (\mathbf{x} - \mathbf{y}))\right) \quad (30)$$

where l is a length-scale of the kernel. The same kernel is applied to find the demixed components for all parameters (time, stimulus, and interaction). I selected the Gaussian kernel so that \mathbf{K} will resemble the graph Laplacian used in the Laplacian eigenmap technique for finding low-dimensional manifolds embedded nonlinearly in a high-dimensional space (Belkin & Niyogi, 2003).

2.3 Simulations

I present simulated populations of $N = 50$ Gaussian neurons that depend linearly on a two-dimensional subspace. For each of S stimulus conditions, the latent trajectory of length T is denoted \mathbf{L}_i which is of size $T \times 2$. The trajectories are approximately smooth in time in the examples explored here. The latent trajectories over all conditions are concatenated as the $M \times 2$, where $M = T \cdot S$, matrix

$$\mathbf{L} = [\mathbf{L}_1^\top, \mathbf{L}_2^\top, \dots, \mathbf{L}_S^\top]^\top. \quad (31)$$

The weights which map the the space of \mathbf{L} to the neural space is $2 \times N$ dimensional matrix \mathbf{W} . For each simulation, the elements of \mathbf{W} are drawn as independent standard normal variables. The observed neural activities are generated by taking

$$\mathbf{X}^* = \mathbf{L}\mathbf{W} + \sigma\mathbf{X}_{noise}, \quad (32)$$

$$\mathbf{X}_{noise(i,j)} \underset{iid}{\sim} \mathcal{N}(0, 1) \quad (33)$$

where \mathbf{X}_{noise} is a $M \times N$ noise term drawn for each simulation. For all simulations, the noise standard deviation was $\sigma = 1$. Finally, the columns of \mathbf{X}^* were z-scored to produce the observation matrix, \mathbf{X} .

In each type of simulation (described in detail in the corresponding Results section), \mathbf{L} is kept constant and the contents of \mathbf{L} is plotted in each simulation section. Across simulations, the weights, \mathbf{W} , and noise, \mathbf{X}_{noise} are sampled independently.

All dPCA and kdPCA fits used a regularization parameter of $\lambda = 1$. The length scale of the Gaussian parameter was fixed to $l = 5$.

The code to generate the simulations and perform all analyses is available publicly at <https://github.com/latimerk/kdpca>.

2.3.1 Assessing demixing performance in simulations

To assess the performance of both dPCA and kdPCA on the simulated datasets, I introduce 2 metrics taken on the neural activity projected onto the first time component and the first stimulus component. These metrics gauge the ability of kdPCA to find parameter-relevant subspaces, instead of only measuring the reconstruction accuracy of \mathbf{X} based on these subspaces.

The performance for time was measured as coefficient of determination between the observations projected into the first time component and time:

$$r_{t,dPCA}^2 = (\text{corr}(\mathbf{X}_{(t,\cdot)}\mathbf{D}_t, t))^2 \quad (34)$$

$$r_{t,kdPCA}^2 = (\text{corr}(\Psi(\mathbf{X}_{(t,\cdot)})\mathbf{G}_t, t))^2 \quad (35)$$

where \mathbf{D}_t and \mathbf{G}_t are column vectors. This measures both how well neural activity is mapped into a 1-dimensional space that depends linearly with time, and how similarly all the stimulus conditions are mapped into this space.

To assess how well the stimulus dimension demixes stimulus conditions, I compute the minimum d' of the observations projected onto the first stimulus dimension (\mathbf{D}_s and \mathbf{G}_s) score between each stimulus condition:

$$d'_{s,dPCA} = \min_{i \neq j} d'(\mathbf{X}_{(\cdot,i)}\mathbf{D}_s, \mathbf{X}_{(\cdot,j)}\mathbf{D}_s), \quad (36)$$

$$d'_{s,kdPCA} = \min_{i \neq j} d'(\Psi(\mathbf{X}_{(\cdot,i)})\mathbf{G}_s, \Psi(\mathbf{X}_{(\cdot,j)})\mathbf{G}_s), \quad (37)$$

$$(38)$$

where $\mathbf{X}_{(\cdot,i)}$ is the set of all observations of stimulus condition i . This metric measures the dependency of time in the stimulus component relative to the mean separation between two stimulus conditions, and takes the worst pairwise case over all stimuli.

Performance was measured on the training conditions alone (training), and the combination of training and test conditions (test).

Unless otherwise indicated, summary statistics of simulation results are shown as $\mu \pm \sigma$ where μ is the mean and σ is the standard deviation across 10000 independently generated simulations.

2.4 Orbitofrontal cortex recordings

I analyzed the trial-averaged response of 214 OFC neurons recorded from 3 rats while the animals performed an odor discrimination task memory task. These data have been reported previously and were obtained from <http://crcns.org> (Kepecs et al., 2008; Uchida et al., 2016). This data set was one of the four examples used by Kobak et al. (2016) to demonstrate dPCA. The data were processed as described by Kobak *et al.* using code made available at <https://github.com/machenslab/elife2016dpca>.

The length-scale parameter of the Gaussian kernel was set to $l = 50$ and a range of regularization parameters settings, λ , was explored.

3 Results

3.1 Example 1: Low-dimensional summation of components

The first simulated example considers a simple case with a linear interaction between stimulus and time (**Fig 3A**). Each 15 time point trajectory follows a simple linear path which is translated in a nearly orthogonal dimension by the stimulus. This scenario is the optimal scenario for dPCA: the latent space can be decomposed linearly into 1 time and 1 stimulus component. Only the training trajectories (marked by circles) were used to fit the dPCA and kdPCA components.

Here, I compare dPCA to kdPCA with both a linear and a Gaussian kernel. The linear kernel is equivalent to performing dPCA (Ψ is the identity function), but provides an alternative formulation that scales with the number of observations, M , rather than the number of neurons, N . This demonstrates that the kdPCA family contains dPCA as a special case.

The activity of the neurons projected onto the first 2 components for each parameter of dPCA and kdPCA are shown in **Fig 3B-D**. The time and stimulus components in both kdPCA and dPCA fall primarily along the first dimension, although kdPCA with the Gaussian kernel shows more modulation in the second stimulus dimension. The interaction dimensions in all 3 methods captures noise in the population activity. The percent of variance of the population activity explained by the 1st stimulus, time, and interaction dimension was nearly identical for all 3

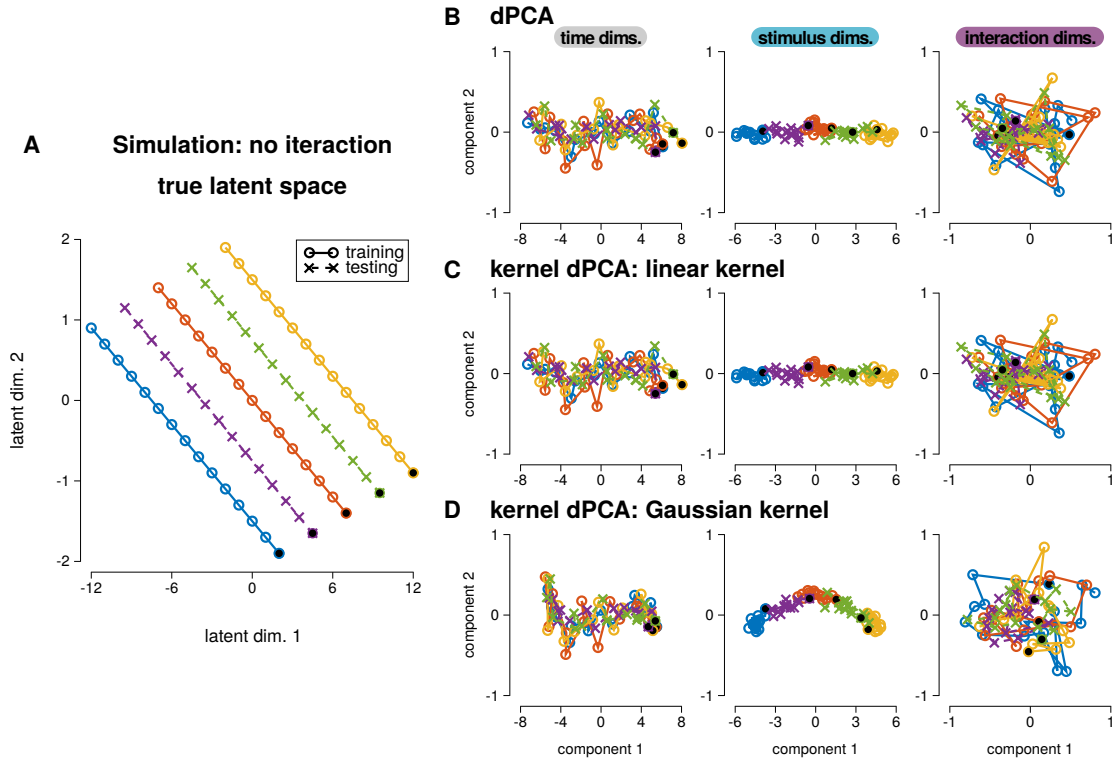


Figure 3: Two dimensional subspace representing latent neural activity as the sum between stimulus condition (indicated by color) and time. **(A)** The true subspace used to generate the simulated neural activity. The circles show trajectories used for finding the low dimensional space, and the crosses indicate test conditions only used to evaluate the estimated components. The black marks denote the time point in each trajectory. **(B)** The simulated activity projected onto the first 2 dPCA components for time (left), stimulus (middle), and interaction (right). **(C)** Same as B for the kdPCA components with a linear kernel. The identical results of B and C demonstrate that linear kdPCA is in fact equivalent to dPCA. **(D)** Same as C for the kdPCA components with a Gaussian kernel.

methods (**Fig 4A,D,G**; time: dPCA = 51.6%, kdPCA_{lin} = 51.6%, kdPCA_{Gauss} = 47.5%; stimulus: dPCA = 46.5%, kdPCA_{lin} = 46.5%, kdPCA_{Gauss} = 42.9%; interaction: dPCA = 1.3%, kdPCA_{lin} = 1.3%, kdPCA_{Gauss} = 1.1%).

To quantify the demixing of the temporal and stimulus components, I examined the activity projected onto the first time component. For the simulation in **Fig 3A**, time and the first demixed component are well correlated for all stimuli (**Fig 4B,E,H left**). Correlating time with the projection across all stimulus conditions measures how the time component maps all stimuli onto a common time-dependent path. For 10000 simulated populations of 50 neurons, all three methods found a time component with strong correlation with time in the 3 training conditions **Fig 4B,E,H right**, training $r_{t,dPCA}^2 = 0.968 \pm 0.011$, $r_{t,kdPCA_{lin}}^2 = 0.968 \pm 0.011$, $r_{t,kdPCA_{Gauss}}^2 = 0.967 \pm 0.008$). These results held up even when the 2 test stimulus trajectories (denoted by crosses) were included (test $r_{t,dPCA}^2 = 0.969 \pm 0.010$, $r_{t,kdPCA_{lin}}^2 = 0.969 \pm 0.010$, $r_{t,kdPCA_{Gauss}}^2 = 0.965 \pm 0.007$).

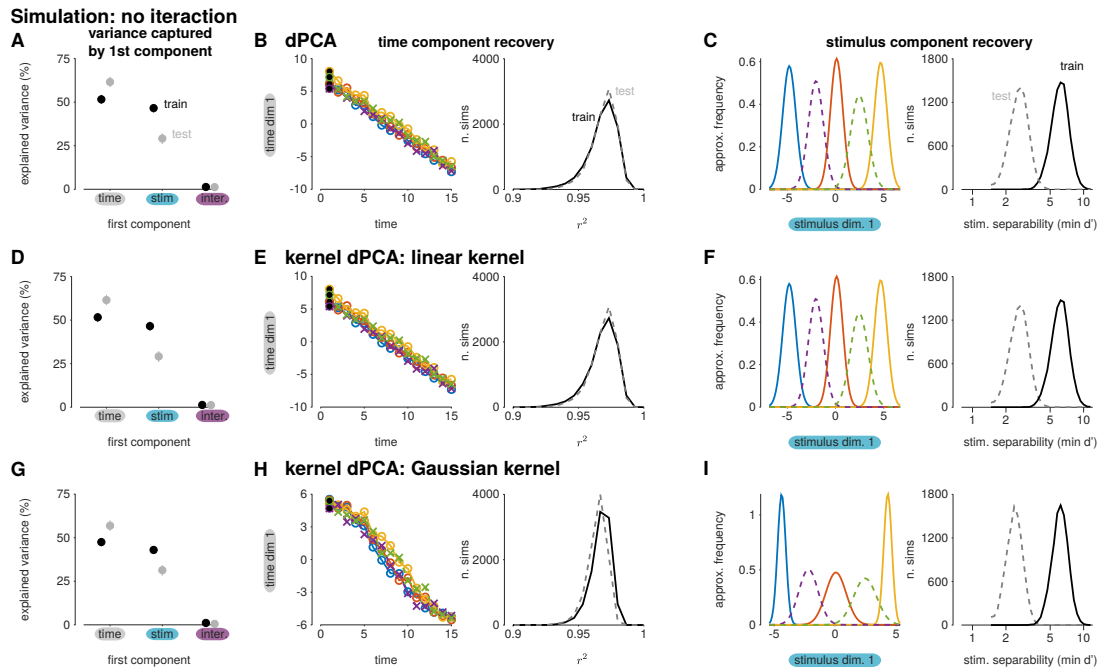


Figure 4: Recovery of time and stimulus with the first components of dPCA and kdPCA for the summed-component simulation in **Fig 3**. **(A)** The mean percent variance explained in the neural activity by the first dPCA time, stimulus, and interaction components. The black points show the percent explained in the training data and the test data are shown in gray. Error bars indicate the 50th percentile region over the 10000 simulations. **(B)** (left) For the example simulation in Fig. 3, the recovered latent trajectory of first time dPCA component as a function of time. (right) Distribution of the r^2 of the first time component with time (squared Pearson's correlation of the two axes in A) for the 10000 simulated neural populations. Solid distribution shows the correlations calculated on the training conditions and the dash distribution shows the correlations for the test conditions. **(C)** (left) For the example simulation in **Fig. 3**, the distribution of neural activity projected onto the first stimulus dPCA component for each stimulus condition approximated by a Gaussian distribution. (right) Quantifying the separability of the stimulus as the minimum d' between each stimulus in the first dPCA stimulus component for the 10000 simulation. Solid distribution shows the separability calculated on the training conditions and the dash distribution shows the separability for the test conditions. **(D-F)** Same as A-C for the first linear kdPCA. **(G-I)** Same as A-C for the first Gaussian kdPCA stimulus component.

I then examined how the first stimulus dimension separated the stimulus conditions across the entire temporal trajectory. For each stimulus, I projected the 15 time points onto the first stimulus dimension. I approximated the distribution on this dimension as a normal distribution (**Fig 4C,F,I left**). If two distributions show little overlap, the two stimulus conditions are separated in the 1st stimulus component across all time points. In contrast, two overlapping distributions would show that the component does not demix time from stimulus successfully. Using d' to quantify the separability of the stimulus conditions across all simulations, each method was able to separate the 3 training stimulus conditions successfully (**Fig 4C,F,I right**;

training $d'_{s,dPCA} = 6.23 \pm 1.13$, $d'_{s,kdPCA_{Gauss}} = 6.23 \pm 1.13$, $d'_{s,kdPCA_{Gauss}} = 6.22 \pm 1.02$). These separability of stimulus category in the first component generalized when including the test stimuli (test $d'_{s,dPCA} = 2.67 \pm 0.52$, $d'_{s,kdPCA_{Gauss}} = 2.67 \pm 0.52$, $d'_{s,kdPCA_{Gauss}} = 2.41 \pm 0.42$); the test conditions lay between the training conditions and thus the separability is expected to go down compared to the training condition.

In summary, both dPCA and kdPCA recovered similar independent stimulus and time dimensions when the simulated activity depended on linearly separable temporal and stimulus components. As expected, kdPCA with a linear kernel produced identical results to dPCA, demonstrating that these two formulations are equivalent (Rodu et al., 2018). With a Gaussian kernel, kdPCA achieved close to the same performance as dPCA (the optimal method for this example).

3.2 Example 2: Rotations

The second example shows a 2-dimensional latent space with stimulus conditions that are rotated around the origin (**Fig 5A**). Each condition is a straight line, but in contrast to the first simulation example, the paths are no longer parallel. This nonlinear interaction creates a potential challenge for finding interpretable subspaces that demix time and stimulus information, despite the fact that the true subspace contains clear structure and separability of components.

I applied dPCA and kdPCA (with a Gaussian kernel) to 10000 simulations of 50 neurons that depended linearly on this subspace (**Fig 5B,D**). The first dPCA and kdPCA components explained on average a similar amount of variance in the data (**Fig 6A**; time: dPCA= 1.8, kdPCA= 1.5; stimulus: dPCA= 33.2, kdPCA= 29.6; interaction: dPCA= 9.2, kdPCA= 6.7). Although kdPCA showed explained less of the variance in the test conditions, indicating that some over fitting occurred (time: dPCA= 0.9, kdPCA= 0.2; stimulus: dPCA= 29.7, kdPCA= 22.3; interaction: dPCA= 7.6, kdPCA= 1.8)). However, the dPCA stimulus components do not clearly demix the stimulus from time, and instead dPCA returns a close reconstruction of the original mixed subspace (**Fig 5B middle**). Thus, the nonlinear interaction between stimulus and time is spread between the stimulus and interaction components. In contrast, the interaction term of kdPCA appears to contain the rotational information : this can be visualized more clearly by summing the stimulus and interaction spaces (**Fig 5E**).

To examine quantitatively the interpretability of the demixed time components, I again correlated time with the activity projected onto the first time component (**Fig 6B,E**). In this example, the dPCA time component failed to show a strong relation to time (training $r^2_{t,dPCA} = 0.102 \pm 0.121$; including test conditions $r^2_{t,dPCA} = 0.058 \pm 0.071$). However, the first time component recovered by kdPCA showed a strong relationship (training $r^2_{t,kdPCA} = 0.655 \pm 0.245$) and the relationship extended to the test examples (test $r^2_{t,kdPCA} = 0.606 \pm 0.224$). To quantify the quality of the stimulus subspace, I again took the minimum d' across stimulus conditions on the first stimulus component (**Fig 6C-F**). In contrast, Gaussian kdPCA showed a higher degree of separation of stimulus conditions than dPCA (training $d'_{s,dPCA} = 1.62 \pm 0.95$, $d'_{s,kdPCA} = 3.14 \pm 1.98$; test $d'_{s,dPCA} = 0.51 \pm 0.42$, $d'_{s,kdPCA} = 1.23 \pm 0.85$).

In this simulation, the demixed components discovered by dPCA differed quantitatively and

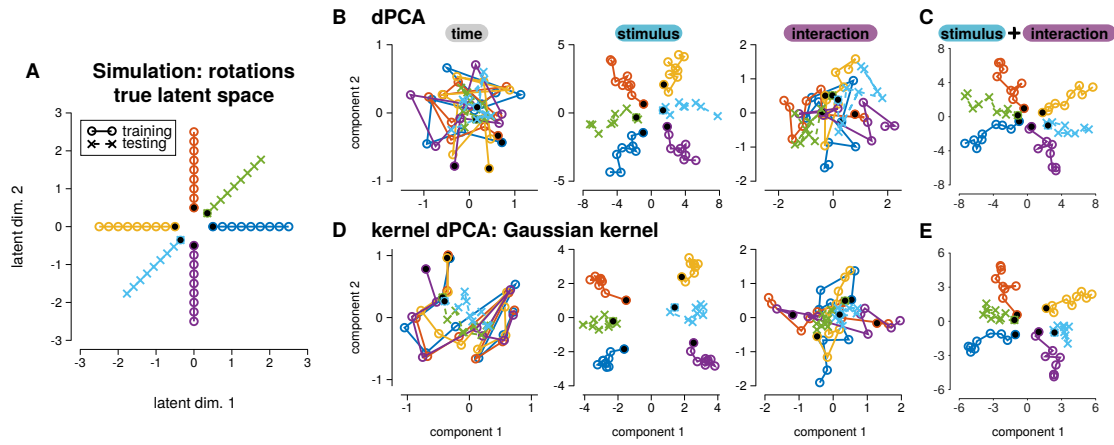


Figure 5: Two dimensional subspace representing latent neural activity for which the trajectories are rotated for each stimulus condition. (A) The true subspace used to generate the simulated neural activity. The circles show trajectories used for finding the low dimensional space, and the crosses indicate test conditions only used to evaluate the estimated components. The black marks denote the time point in each trajectory. (B) The simulated activity projected onto the first 2 dPCA components for time (left), stimulus (middle), and interaction (right). (C) The sum of the stimulus and interaction components (i.e., component 1 is the sum of the projection onto the first stimulus component and the projection onto the first interaction component). (D-E) Same as B-C for the kdPCA components with a Gaussian kernel.

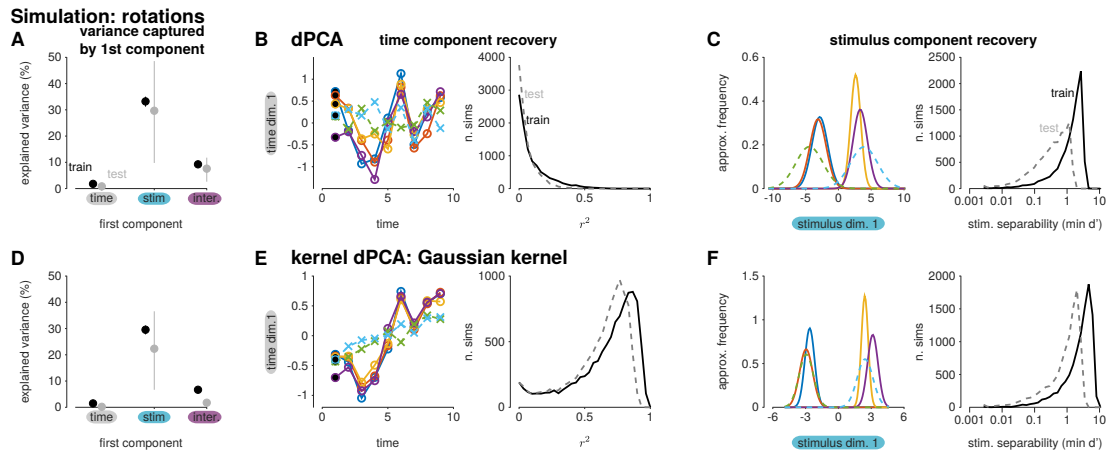


Figure 6: Recovery of time and stimulus with the first components of dPCA and kdPCA for the stimulus-dependent rotation simulation in Fig 5. (A-C) Analyses of the dPCA of the rotation simulation. Figures follow the structure as Fig. 4A-C. (D-F) Same as A-C for Gaussian kdPCA of the rotation simulation.

qualitatively from the components derived by kdPCA (with a Gaussian kernel). The time components recovered by dPCA and kdPCA explain a similarly negligible percent of the simulated neural activity when projected linearly into the high-dimensional neural space. However, kdPCA reliably discovers a nonlinear component that contains information about time in the

simulated neural activity.

3.3 Example 3: Scaling

In the final simulation, the 2-dimensional latent space contained conditions that were scaled differently across stimulus conditions (**Fig 7A**). In this example, the temporal and stimulus components are in a separable 2-dimensional manifold that is embedded nonlinearly within the 2-dimensional space. Applying dPCA to simulated neural responses shows time and interaction components that recover the shape of the true subspace (**Fig 7B**). In contrast, Gaussian kdPCA shows a time component that squeezes the different stimuli together (**Fig 7D**). The kdPCA interaction component reflects the nonlinear embedding: the gold and blue traces - the largest and smallest components respectively - are the largest two traces in the interaction space. In the 2-dimension interaction space, the orientations of the gold and blue traces are flipped corresponding to the relative shrinking of the blue trace and stretching of the gold. The red condition, which is the mean of all the conditions, projects around the origin of the interaction component. Taking the sum of the interaction and time spaces shows that the kdPCA interaction components indeed scale the time trace for each stimulus condition (**Fig 7E**).

I again analyzed the demixing performance of the first time and stimulus dimension of both techniques. Each stimulus projected onto the first dPCA time component is well correlated with time, but the slope varies across stimulus conditions (**Fig 8B**; training $r_{t,dPCA}^2 = 0.865 \pm 0.009$; test $r_{t,kdPCA}^2 = 0.891 \pm 0.008$). The kdPCA time component again shows a strong correlation with time, but the time component shows less dependence on the stimulus condition (**Fig 8E**; training $r_{t,kdPCA}^2 = 0.967 \pm 0.013$; test $r_{t,kdPCA}^2 = 0.970 \pm 0.013$). Separability of the stimulus conditions was also far better in the first kdPCA stimulus component than in the dPCA component (**Fig 8E**; training $d'_{s,dPCA} = 0.85 \pm 0.38$, $d'_{s,kdPCA} = 6.35 \pm 0.48$; test $d'_{s,dPCA} = 0.38 \pm 0.34$, $d'_{s,kdPCA} = 2.81 \pm 0.26$).

The dPCA first components explained a higher percent of the variance of the training data (**Fig 8A,D**; time: dPCA= 56.9%, kdPCA= 49.3%; stimulus: dPCA= 19.9%, kdPCA= 13.2%; interaction dPCA= 15.0%, kdPCA= 8.2%) and the test data (time: dPCA= 60.4%, kdPCA= 57.5%; stimulus: dPCA= 16.7%, kdPCA= 7.4%; interaction dPCA= 15.9%, kdPCA= 2.6%) than the kdPCA components. However, these results taken together indicate that the lack of demixing in the dPCA components could inflate the percent explained by the individual parameters: the first two dPCA time components reconstruct the original 2-D latent space which includes stimulus-time interactions. Thus, instead of recovering the 2-D subspace in **Fig 7A**, kdPCA recovers a nonlinearly embedded manifold in which time and stimulus are the natural coordinates.

3.4 Example 4: Isolating decision-related activity in rat OFC

I analyzed one of the datasets used by (Kobak et al., 2016) to demonstrate dPCA for extracting stimulus- and decision- related activity in a large population of neurons. This analysis included 214 neurons from rat OFC during an odor categorization task (**Fig 9A**). In this task, the rats

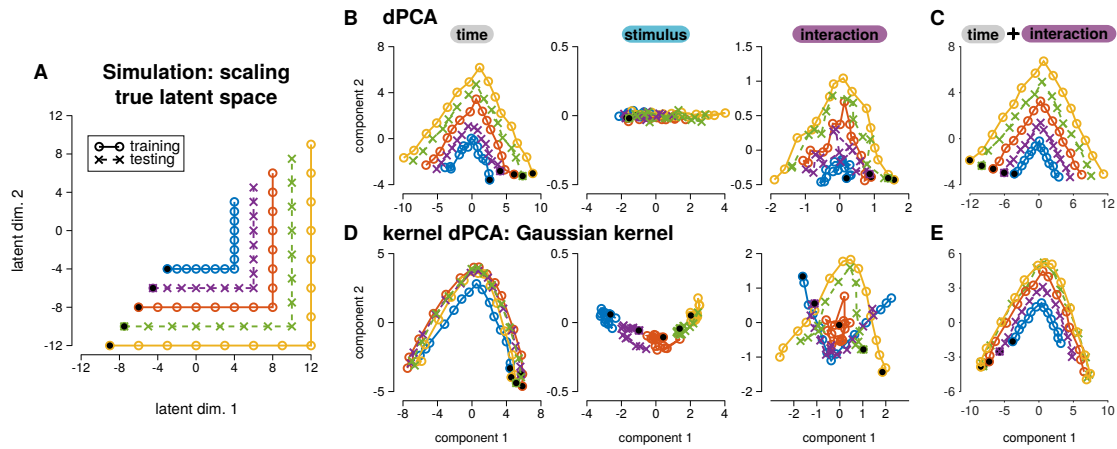


Figure 7: Two dimensional subspace representing latent neural activity for which the trajectories are scaled for each stimulus condition. (A) The true subspace used to generate the simulated neural activity. The circles show trajectories used for finding the low dimensional space, and the crosses indicate test conditions only used to evaluate the estimated components. The black marks denote the time point in each trajectory. (B) The simulated activity projected onto the first 2 dPCA components for time (left), stimulus (middle), and interaction (right). (C) The sum of the time and interaction components (i.e., component 1 is the sum of the projection onto the first time component and the projection onto the first interaction component). (D-E) Same as B-C for the kdPCA components with a Gaussian kernel.

were presented with a mixture of 2 odorants. The relative concentration of the odorants varied over trials. The rats were trained to indicate which odorant was strongest by a nose poke into the left or right choice port. I analyzed the trial-averaged activity under 8 conditions covering 4 concentration levels for the 2 possible decisions. The two easiest conditions (the 100% concentration) in which the rats performed nearly perfectly, were used only as test conditions and were thus not used to fit dPCA or kdPCA (as was done in Kobak *et al.*). I fit dPCA and kdPCA to these data and found qualitatively similar components (Fig 9B-C). Each component captured a similar amount of variance. However, the first 2 dPCA components captured a total of approximately 1.6% more variance in the training data and 2.8% more variance of the test data across a range of regularization parameter settings (Fig 9D).

Here I focus on the ability of kdPCA to isolate (demix) the decision-related activity from stimulus-dependent responses. Figure 6B in Kobak *et al.* indicates that some stimulus-dependence remains in the decision terms, and my application of dPCA showed the same results (Fig 9B 3rd row). Although decisions depend on the stimulus, these dependencies should ideally be confined to the interaction term. Thus, the stimulus and decision terms are not completely demixed by dPCA..

To quantify the stimulus-dependence in the decision components of dPCA and kdPCA, I compared the activity projected onto the first decision component for each stimulus (traces of Fig 9B 3rd row) to the average decision component of the other stimulus conditions. For each stimulus level, s , the vector d_s contains the traces of the activity projected onto the first

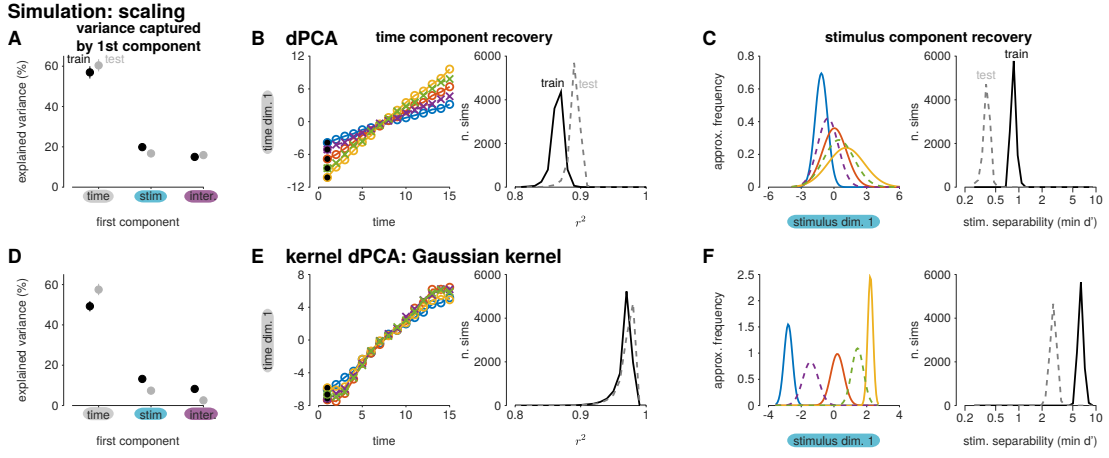


Figure 8: Recovery of time and stimulus with the first components of dPCA and kdPCA for the stimulus-dependent scaling simulation in Fig 7. (A-C) Analyses of the dPCA of the scaling simulation. Figures follow the structure as Fig. 4A-C. (D-F) Same as A-C for Gaussian kdPCA of the scaling simulation.

decision component for both left and right choices (concatenated):

$$\mathbf{d}_s^{dPCA} = [(\mathbf{X}_{(\cdot,s,d=left)} \mathbf{D}_d)^\top \quad (\mathbf{X}_{(\cdot,s,d=right)} \mathbf{D}_{d,1})^\top]^\top \quad (39)$$

$$\mathbf{d}_s^{kdPCA} = [(\mathbf{K}_{(\cdot,s,d=left)} \mathbf{Z}_d)^\top \quad (\mathbf{K}_{(\cdot,s,d=right)} \mathbf{Z}_{d,1})^\top]^\top \quad (40)$$

where $\mathbf{X}_{(\cdot,s,d=left)}$ (or $\mathbf{K}_{(\cdot,s,d=left)}$) indexes the rows of \mathbf{X} containing all time points for stimulus s and the left choice. For the test conditions, the columns of $\mathbf{K}_{(\cdot,s,d=left)}$ are computed as in Eq. 28. The stability in the training data is computed as the average R^2 between \mathbf{d}_s for each training s and the mean \mathbf{d}_s of the remaining stimuli. The stability in the test data is the average R^2 of the 2 test conditions predicted by the mean \mathbf{d} of the training conditions:

$$R_{train}^2 = \frac{1}{4} \sum_{s \in train} \left(1 - \frac{(\mathbf{d}_s - \langle \mathbf{d}_j \rangle_{j \in train, j \neq s})^2}{(\mathbf{d}_s - \bar{\mathbf{d}}_s)^2} \right) \quad (41)$$

$$R_{test}^2 = \frac{1}{2} \sum_{s \in test} \left(1 - \frac{(\mathbf{d}_s - \langle \mathbf{d}_j \rangle_{j \in train})^2}{(\mathbf{d}_s - \bar{\mathbf{d}}_s)^2} \right) \quad (42)$$

The stability computed over a range of settings of the regularization parameter is shown in Fig 9F. The kdPCA decision component, while similar in shape to its dPCA counterpart, shows greater stability across stimuli in both the training and test conditions. Setting λ to achieve the maximum test set stability, dPCA's stability is $R_{train}^2 = 0.965$ and $R_{test}^2 = 0.940$ while the kdPCA training stability is $R_{train}^2 = 0.996$ and $R_{test}^2 = 0.977$. The decision-related activity of the first dPCA explained only 0.15% more variance than the kdPCA component, and kdPCA explained 1.1% more of the variance in the test conditions (Fig 9E). Thus, kdPCA finds a more demixed representation of the neural data which shows superior generalization performance than the linear components recovered by dPCA.

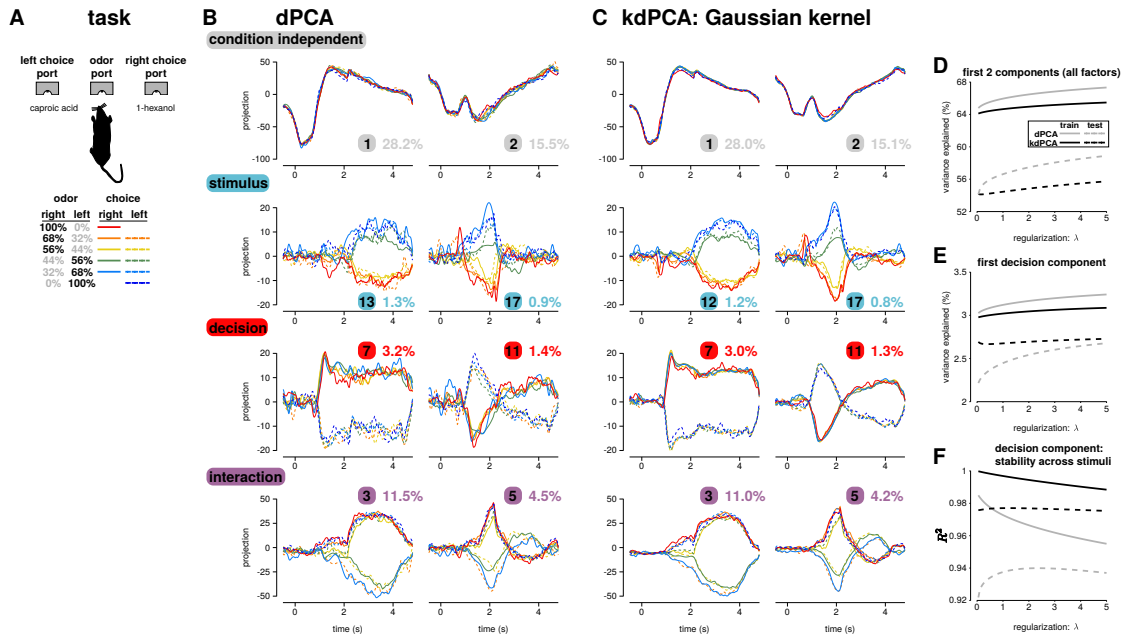


Figure 9: dPCA and kdPCA produce similar results in reducing the dimensionality of data recorded from 214 neurons in rat OFC from Kepecs et al. (2008). **(A)** The rat categorizes concentrations of two odors (caproic acid and 1-hexanol) and signals choice by selecting the left or right choice port. **(B)** The average neural activity projected onto the first 2 dPCA condition independent, stimulus, decision, and stimulus-decision interaction components as a function of time in the trial. The percent variance explained and the component’s rank (from most variance explained to least) is given in each plot. **(C)** The same as B for the Gaussian kdPCA components. **(D)** The percent variance explained in the training data (solid lines) and test data (dashed lines) as a function of the regularization parameter λ by the sum of the first two components for all factors (i.e., sum all the components shown in panels B-C) for dPCA (gray) and kdPCA (black). **(E)** The percent variance explained in the training data (solid lines) and test data (dashed lines) as a function of the λ by the first decision component (row 3 left of panels B-C) for dPCA (gray) and kdPCA (black). **(F)** The stability factor of the first decision component for the 4 training stimulus conditions (solid lines) and 2 test conditions (dashed lines) as a function of the regularization parameter λ . Higher values indicate less stimulus-dependence of the decision-only component.

4 Discussion

Here, I have proposed an extension to dPCA that can extract nonlinear, but still low-dimensional, components from neural populations which are related to experimental parameters. The resulting components provide a more demixed reduced representation of the data when nonlinear interactions occur in the data.

I validated kdPCA in simulations by recovering relevant demixed components when the true components are scaled by a gain factor or rotated under different conditions. The dPCA components recovered from the simulated activity were less associated with the experimental pa-

rameters of interest than the kdPCA components. In the scaling and rotations simulations, dPCA recovered the original *mixed* dimensions, and thus failed to go beyond standard PCA. The lack of demixing could potentially bias estimates of the variance explained in the data by each component. In contrast, kdPCA successfully recovered demixed stimulus and time components. Although nonlinear components can be more difficult to interpret than linear components, the variable-dependent reconstructions in kdPCA must sum together to approximate the complete neural response. As a result, stimulus-dependent scaling and rotation could still be visualized in the interaction terms in the simulations explored here.

In data recorded from rat OFC during a decision-making task, I showed that kdPCA could extract decision-dependent components that were more independent across stimulus conditions than dPCA. Additionally, the nonlinear demixed components generalized more successfully to test conditioned than the linear components. These results show that nonlinear interactions were present between stimulus and decision in this data set that could not be fully demixed by linear methods.

The kernel formulation with a linear kernel provides an alternative formulation of dPCA that scales in the number of observations, not the number of neurons. This scaling could aid in finding linear components as the number of recorded neurons in a single experiment grows (Stevenson & Kording, 2011; Hainmueller & Hazlett, 2014; Kobak et al., 2016). Additionally, in the case where components could be linearly demixed, I found that Gaussian kdPCA produces similar results.

The flexibility of kdPCA requires tuning more free parameters than dPCA. Like dPCA, kdPCA requires selecting a regularization term. In addition, the user must also choose an appropriate kernel, and select any parameters of the kernel (e.g., bandwidth). The same crossvalidation procedure recommended by Kobak et al. (2016) could be applied to kdPCA. Additionally, future work could treat the demixing problem within a probabilistic model, for instance as an extension of Gaussian process factor analysis (Yu et al., 2009). The Gaussian process framework could then be leveraged to select hyperparameters.

In summary, visualizing the complex responses of large neural populations to yield insights about neural dynamics and processing will require nonlinear dimensionality reduction techniques (Stopfer et al., 2003; Cunningham & Byron, 2014; Gallego et al., 2017). kdPCA is one such tool that may aid investigators seeking to unravel neural manifolds.

Acknowledgments

I thank David Freedman, Leor Katz, Jonathan Pillow, Benjamin Scholl, and Jacob Yates for their helpful comments. This work was supported by a Chicago Fellowship.

References

- Belkin, M., & Niyogi, P. (2003). Laplacian eigenmaps for dimensionality reduction and data representation. *Neural computation*, *15*(6), 1373–1396.
- Cunningham, J. P., & Byron, M. Y. (2014). Dimensionality reduction for large-scale neural recordings. *Nature neuroscience*, *17*(11), 1500.
- Gallego, J. A., Perich, M. G., Miller, L. E., & Solla, S. A. (2017). Neural manifolds for the control of movement. *Neuron*, *94*(5), 978–984.
- Gao, P., & Ganguli, S. (2015). On simplicity and complexity in the brave new world of large-scale neuroscience. *Current opinion in neurobiology*, *32*, 148–155.
- Hainmueller, J., & Hazlett, C. (2014). Kernel regularized least squares: Reducing misspecification bias with a flexible and interpretable machine learning approach. *Political Analysis*, *22*(2), 143–168.
- Haroon, D. R., Szedmak, S., & Shawe-Taylor, J. (2004). Canonical correlation analysis: An overview with application to learning methods. *Neural computation*, *16*(12), 2639–2664.
- Kepecs, A., Uchida, N., Zariwala, H. A., & Mainen, Z. F. (2008). Neural correlates, computation and behavioural impact of decision confidence. *Nature*, *455*(7210), 227.
- Kobak, D., Brendel, W., Constantinidis, C., Feierstein, C. E., Kepecs, A., Mainen, Z. F., Qi, X.-L., Romo, R., Uchida, N., & Machens, C. K. (2016). Demixed principal component analysis of neural population data. *Elife*, *5*, e10989.
- Lai, P. L., & Fyfe, C. (2000). Kernel and nonlinear canonical correlation analysis. *International Journal of Neural Systems*, *10*(05), 365–377.
- Rodu, J., Klein, N., Brincat, S. L., Miller, E. K., & Kass, R. E. (2018). Detecting multivariate cross-correlation between brain regions. *Journal of neurophysiology*.
- Schölkopf, B., Smola, A., & Müller, K.-R. (1998). Nonlinear component analysis as a kernel eigenvalue problem. *Neural computation*, *10*(5), 1299–1319.
- Stevenson, I. H., & Kording, K. P. (2011). How advances in neural recording affect data analysis. *Nature neuroscience*, *14*(2), 139.
- Stopfer, M., Jayaraman, V., & Laurent, G. (2003). Intensity versus identity coding in an olfactory system. *Neuron*, *39*(6), 991–1004.
- Uchida, N., Kepecs, A., Zariwala, H. A., & Mainen, Z. F. (2016). Single-neuron spike train recordings from rat orbitofrontal cortex during an odor classification task. CRCNS.org <http://dx.doi.org/10.6080/K0FT8HZ2>.
- Williams, A. H., Kim, T. H., Wang, F., Vyas, S., Ryu, S. I., Shenoy, K. V., Schnitzer, M., Kolda, T. G., & Ganguli, S. (2018). Unsupervised discovery of demixed, low-dimensional neural dynamics across multiple timescales through tensor component analysis. *Neuron*.

Williamson, R. C., Doiron, B., Smith, M. A., & Byron, M. Y. (2018). Bridging large-scale neuronal recordings and large-scale network models using dimensionality reduction. Tech. rep., PeerJ Preprints.

Yu, B. M., Cunningham, J. P., Santhanam, G., Ryu, S. I., Shenoy, K. V., & Sahani, M. (2009). Gaussian-process factor analysis for low-dimensional single-trial analysis of neural population activity. *Journal of Neurophysiology*, *102*(1), 614–635. PMID: 19357332.